Truncation Artifact Reduction Based on Big Data: A Preliminary Study

Yanbo Zhang and Hengyong Yu*

***Abstract*–In X-ray CT, projections are sometimes truncated due to size mismatches between small detectors and/or large objects, which introduce truncation artifacts in reconstructed images. In this work, we aim at addressing the truncation problem using the idea of "big data"-aided analysis/synthesis. For a specific cross-section position of a patient, e.g., pelvis in this paper, we collect hundreds CT images to build a database. We propose the "image-sum" as the feature of each image in the database. With this feature, we can find the most relevant image to the truncated projection from the database. Finally, the forward projections of the selected image are used to extend truncated projections. The experimental results show that the proposed method can reduce the truncation artifacts successfully.**

***Keywords*—Computed tomography; truncation artifacts; big data; projection extension.**

I. Introduction

In some imaging cases, the CT scan field of view (FOV) cannot cover all the parts of imaging objects, causing truncation in the projection domain. This leads to bright truncation artifacts in the images directly reconstructed by the conventional filtered backprojection (FBP) algorithm, and the image quality is significantly affected.

So far, various techniques have been proposed to deal with the data truncation problem. Data truncation can be viewed as the interior tomography, and the region-of-interest (ROI) can be iteratively reconstructed [1, 2]. Although the image in a ROI can be accurately obtained, it is time-consuming and has not been applied in commercial CT. A major class of practical approaches is to extend the truncated projections based on extrapolation. Hsieh *et al.* assumed the cross-section of a patient as a water cylinder, and used the magnitudes and slopes of the projections at the location of truncation to estimate the missing projections [3]. Later, a better performance was achieved by replacing the water cylinder fit with a Gaussian extrapolation [4, 5]. Maltz *et al.* approximated the thickness of the patient along the projection rays by calculating water-equivalent thicknesses to estimate the truncated data [6]. However, it might lead to inaccuracy estimation for non-water tissues. Recently, Xia *et al.* proposed another water cylinder extrapolation based algorithm. In their work, two nontruncated fluoroscopic images were adopted and the patient-specific *a priori* shape was used to estimate the missing projections more precisely [7]. By comparison, Kolditz *et al.* [8] obtained patient size and shape information from a nontruncated low-dose CT scan for projection extrapolation. With the help of those additional information, these methods achieved excellent performance in terms of artifacts reduction. However, the requirement of additional information usually limits their practical applications.

The above analysis suggests that introducing *a priori* information benefits the extrapolation. Different from the aforementioned methods, in this work, we try to explore the additional information from "big data". To achieve this goal, a database consisting of various CT images is built, and then a way is developed to select a proper image to assist estimating the missing projection data.

*This work was supported in part by NIH/NIBIB U01 grant EB017140 and R21 grant EB019074. Y.B. Zhang and H.Y. Yu are with the Department of Electrical and Computer Engineering, University of Massachusetts Lowell, Lowell, MA 01854, USA. Corresponding author: H.Y. Yu (e-mail: hengyong-yu@ieee.org).

II. Methods

Due to the similarity of human anatomy structures, for a given cross-section position, the distributions of tissues are usually similar among different patients in clinical CT images. As a result, it is reasonable to find another patient's CT image that is similar to the truncated data, and the forward projection of this image (referred as to the reference image) can be applied to extend the truncated data. The key point of this idea is how to find such a similar image to a specific truncated data. For this purpose, we build a database consisting of CT images at a specific position (e.g., pelvis in this paper). We also propose two terms the "image-sum" and the "projection-sum" to evaluate the similarity of a CT image in the database and the truncated data. Finally, the most similar image is selected as the reference image.

A. Build a Database

Because pelvic CT images have higher probability to suffer from truncation, we build a database consisting of pelvic CT images to demonstrate our idea. To be a qualified image in the database, all the tissues should be covered by the image so that the entire cross-section information is included.

We introduce the "image-sum" as a feature of each image, and Fig. 1 depicts how to compute this feature. As shown in Fig. 1, the radius of FOV is defined as R, and L_k is a line passing through the system center along the angle β_k. In addition, μ_i is the linear attenuation coefficient of an arbitrary pixel in the CT image, and d_{ik} represents the distance from the pixel μ_i to the line L_k. Let Φ_k be the set of pixels whose distances to L_k are smaller than R, namely, $\Phi_k = \{i: d_{ik} \leq R\}$. Given a group of angles $\beta = [\beta_1, \beta_2, \cdots, \beta_k, \cdots, \beta_K]$, the image-sum vector of the t[th] CT image is denoted as $\phi^t = [\phi_1^t, \phi_2^t, \cdots, \phi_k^t, \cdots, \phi_K^t]$ and computed as

$$\phi_k^t = \frac{\sum_{i \in \Phi_k} \mu_i}{s^2}, \quad (1)$$

where s is pixel size of the CT image. The denominator of Eq.(1) is used for normalization.

B. Find a Reference Image from the Database

The obtained truncated projection is denoted as p^{tr}, which is rebinned to parallel projections p^{para}. The detector bin length of parallel projections is b. The parallel projection is also bounded by the FOV as shown in Fig. 2. The projection-sum at the angles $\beta = [\beta_1, \beta_2, \cdots, \beta_k, \cdots, \beta_K]$ is denoted as $\psi = [\psi_1, \psi_2, \cdots, \psi_k, \cdots, \psi_K]$, which is computed as

$$\psi_k = \frac{\sum p_{\beta_k}^{para}}{b}, \tag{2}$$

where $p_{\beta_k}^{para}$ is the vector of parallel projections at the angle of β_k, and $\sum p_{\beta_k}^{para}$ means the summation of these measurements. It is clear that the meanings of image-sum and projection-sum are identical, and both of them represent the summation of the image pixels along a given angle and bounded by the FOV. To find the closest image to the truncated data, we compare the ϕ^t and ψ as follows,

$$t^* = \arg\min_t \|\psi - \phi^t\|_2^2, \tag{3}$$

where t^* is the index of the most similar image. In our implementation, $\|\psi - \phi^t\|_2^2$ is computed with respect to each image in the database, and the image with the smallest $\|\psi - \phi^t\|_2^2$ is selected as the reference image.

Because CT data are untruncated in the database, it is not applicable to patients who are not fully covered by the FOV of existing CT scanners. Hence, an adaptive scaling is introduced to obtain a suitable reference image. Therefore, we have

$$t^* = \arg\min_t \|\psi - a^t\phi^t\|_2^2, \tag{4}$$

where $a^t = \sum_k \psi_k / \sum_k \phi_k^t$ is a scaling factor, and the image selected from the database is scaled according to the factor a^t.

C. Extend Truncated Projections

The forward projection p^{ref} of the reference image is obtained in the same CT geometry as that for the truncated projection p^{tr}, but with a larger number of detector bins so that the entire reference image is covered in the enlarged FOV. The numbers of detector bins of p^{tr} and p^{ref} are denoted as N^{tr} and N^{ref}, respectively.

Fig. 3 depicts the method to obtain p^{ex} from p^{tr} and p^{ref}. As shown in Fig. 3(a), for a given projection view, differences of the two projections at the truncated boundaries are Δ_1 and Δ_2, respectively. These obvious disconnections may introduce artifacts in the reconstructed images. Hence, it is necessary to introduce a new projection p^{diff} for smooth transition. As illustrated in Fig. 3(b), the projection differences reduce gradually from the truncation boundaries to the two ends of the extended projection. Then, the extended projection p^{ex} at a specific view is given as below

$$p_j^{ex} = \begin{cases} p_j^{tr}, & j \in \Omega \\ p_j^{ref} + p_j^{diff}, & otherwise \end{cases}, \tag{5}$$

where Ω is the set of indexes of available measurements in the projection. Finally, the corrected image is reconstructed from the extended projection using FBP.

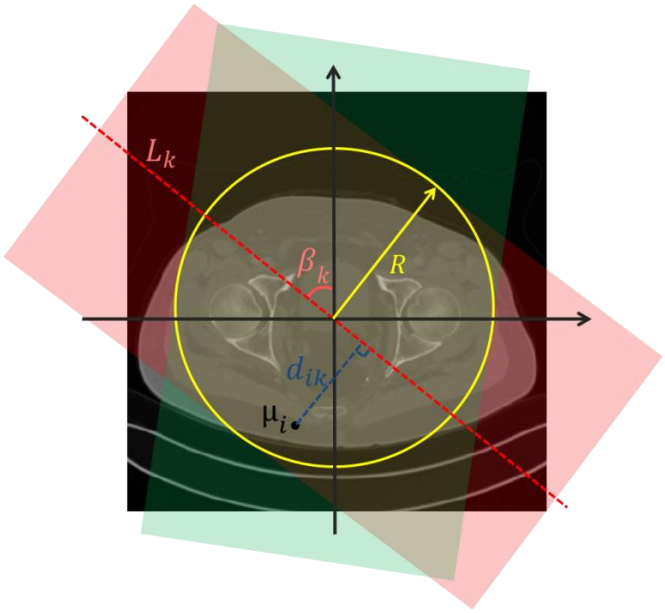

Fig. 1. Computation of the image-sum at a specific angle. The yellow circle indicates the FOV of CT scan. The boundaries of the red and green rectangular regions are tangent to the circle, and along the specific angles. L_k is the central line of red rectangle of the angle β_k. μ_i is an arbitrary pixel in the CT image, and d_{ik} represents distance from the pixel μ_i to the line L_k. The image-sum along a specific angle is computed by summing the CT image pixel values in the overlapped region of the rectangle at the angle and the CT image.

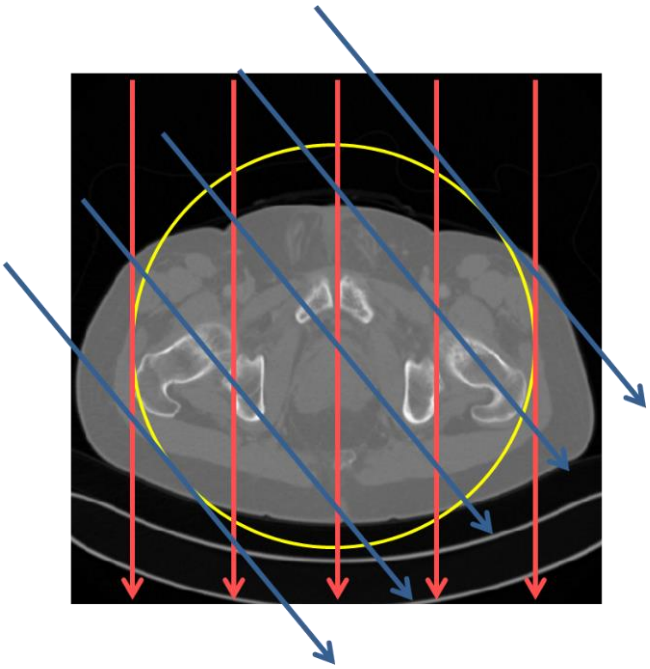

Fig. 2. Computation of the projection-sum at a specific angle. The yellow circle indicates the FOV of CT scan. After rebinning, the parallel projections are obtained and the boundary projection rays are tangent to the FOV circle.

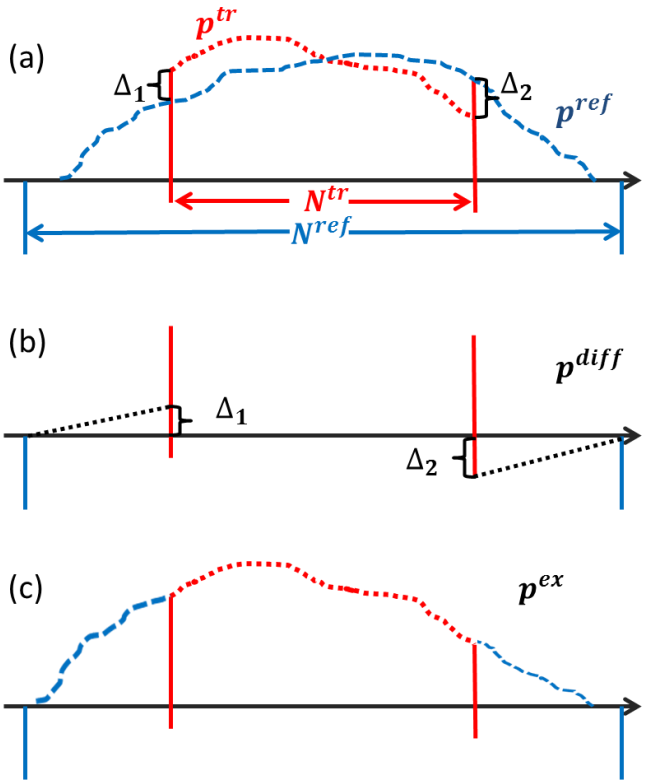

Fig. 3. Illustration of the projection extension. (a) For a specific view, the projections of p^{tr} and p^{ref} are plotted in red and blue curves, respectively; (b) the black dot-curves p^{diff} is used for smooth transition between p^{tr} and p^{ref} at the truncation boundaries; (c) the final extended projection p^{ex}.

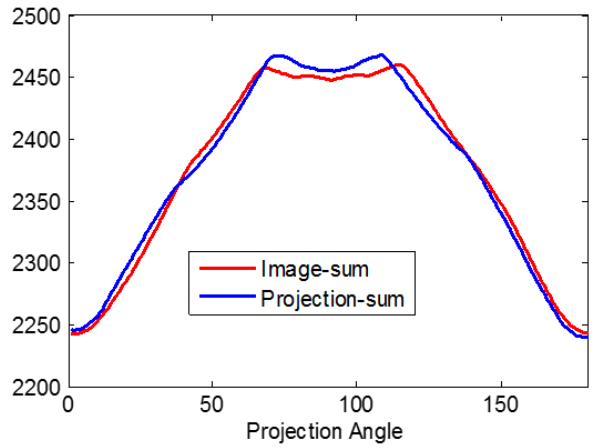

Fig. 6. Plots of the image-sum and the projection-sum. The horizontal axis indicates the projection angles in the range of [0 179], and the vertical axis means the values of the image-sum and projection-sum.

III. Experimental Results

In this work, we build a pelvic CT image database, which contained 790 images from 9 patients. These images are all collected from a SIEMENS SOMATOM Definition Flash CT scanner. All the images are reconstructed at 3mm slice thickness, each image consists of 512×512 pixels, and each pixel covers an area of 0.7422×0.7422 mm^2. The number of elements in the image-sum vector is 180 with an angle interval of 1°. Several samples of the CT images in the database are shown in Fig. 4.

To validate the effectiveness of the proposed method, a pelvic CT image is used to generate projections, and the patient of this image is not included in the dataset. In this test, an equidistant fan-beam geometry is assumed [9]. The source-to-center distance and the source-to-detector distance are 595 mm and 1085.6 mm, respectively. The view number is 984 over a full scan. There are 920 detector bins, the bin width is 1 mm, and only 530 detector bins are assumed available to simulate the truncation case. The reconstructed images have 512×512 pixels each of which covers an area of 0.7422×0.7422 mm^2.

In this experiment, Gaussian extrapolation [4, 5] is implemented as a competing method. The experimental results are shown in Fig. 5. The ground truth image is shown in Fig. 5(a). The image reconstructed from truncated projections by FBP is given in Fig. 5(b), in which the FOV is highlighted with a yellow circle and bright truncation artifacts are very strong near the circle. The image corrected using Gaussian extrapolation is shown in Fig. 5(c) where artifacts are reduced significantly. The reference image selected from the database is presented in Fig. 5(b). Fig. 6 depicts the plots of the image-sum and projection-sum of Fig. 5(d) and Fig. 5(a), respectively, and the red curve is the one in the database closest to the blue curve. Although density distributions in Figs. 5(a) and 5(d) are different, the patients' size and shape are similar. After the correction using the proposed algorithm, truncation artifacts are reduced completely and part of the image information out of the FOV is restored. To quantitatively evaluate the performance for artifact reduction, the root mean squared error (RMSE) in the FOV is computed. RMSEs of uncorrected, Gaussian extrapolation and the proposed method are 215 HU, 28 HU and 12 HU, respectively.

IV. Discussion And Conclusion

In this preliminary study, the number of images in the database is only 790, which is not sufficient as "big data". To this point, it is possible to access CT images from internet to increase the size of datasets. Once various CT image cases are included, it intends to find a reference image that is extremely similar to the truncated image, which in turn improves the performance of projection extension.

In this work, all the images in the database are from the same CT scanner. To involve as many CT images as possible, data may come from difference sources. Hence, these images may have different parameters, such as image size, pixel size, tube energies, patient positions, *etc*. These factors need to be considered in the construction of a dataset.

In conclusion, we have presented a big data based method to address the projection truncation problem. A reference image is selected from the database, and then the forward projection of this reference image is used to extend the

truncated projection. Our experimental results show that the artifacts are reduced significantly and the image information outside the FOV is restored to some extent.

REFERENCES

[1] H. Y. Yu and G. Wang, "Compressed sensing based interior tomography," *Physics in Medicine and Biology*, vol. 54, pp. 2791-2805, 2009.

[2] G. Wang and Y. H. Yu, "The meaning of interior tomography," *Physics in Medicine and Biology*, vol. 58, p. R161, 2013.

[3] J. Hsieh, E. Chao, J. Thibault, B. Grekowicz, A. Horst, S. McOlash, and T. J. Myers, "A novel reconstruction algorithm to extend the CT scan field-of-view," *Medical Physics*, vol. 31, pp. 2385-2391, 2004.

[4] M. Zellerhoff, B. Scholz, E.-P. Ruehrnschopf, and T. Brunner, "Low contrast 3D reconstruction from C-arm data," in *SPIE Medical imaging*, 2005, pp. 646-655.

[5] S. Hoppe, J. Hornegger, G. Lauritsch, F. Dennerlein, and F. Noo, "Truncation correction for oblique filtering lines," *Medical physics*, vol. 35, pp. 5910-5920, 2008.

[6] J. S. Maltz, S. Bose, H. P. Shukla, and A. R. Bani-Hashemi, "CT Truncation artifact removal using water-equivalent thicknesses derived from truncated projection data," in *the 29th Annual International Conference of the IEEE Engineering in Medicine and Biology Society*, 2007, pp. 2907-2911.

[7] Y. Xia, S. Bauer, A. Maier, M. Berger, and J. Hornegger, "Patient-bounded extrapolation using low dose priors for volume-of-interest imaging in C-arm CT," *Medical physics*, vol. 42, pp. 1787-1796, 2015.

[8] D. Kolditz, Y. Kyriakou, and W. Kalender, "Volume-of-interest (VOI) imaging in C-arm flat-detector CT for high image quality at reduced dose," *Medical physics*, vol. 37, p. 2719, 2010.

[9] B. De Man and S. Basu, "Distance-driven projection and backprojection in three dimensions," *Physics in Medicine and Biology*, vol. 49, pp. 2463-2475, 2004.

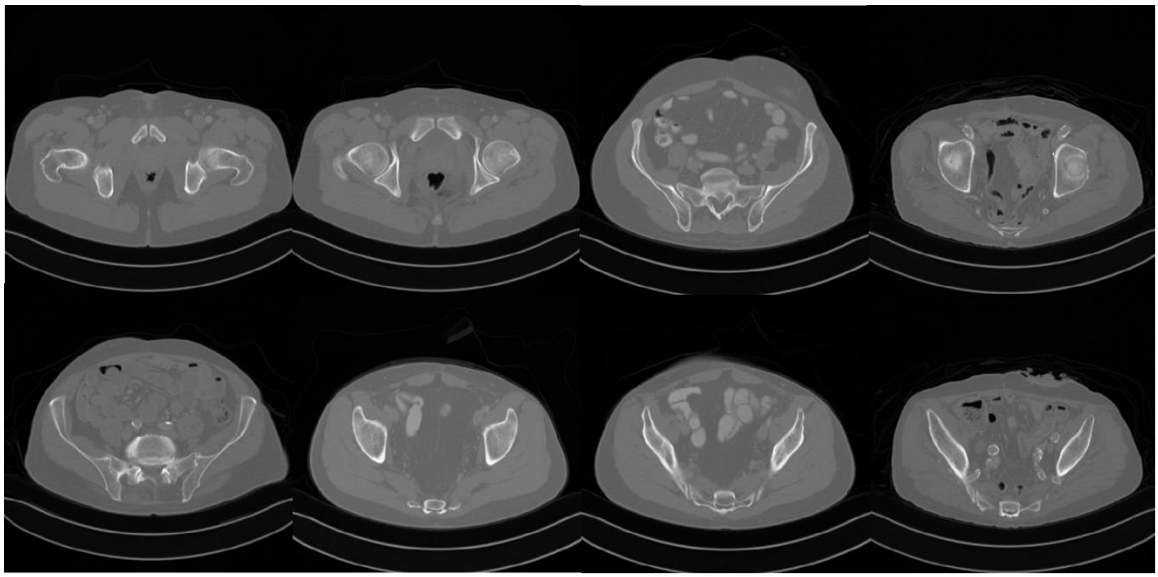

Fig.4. Samples of CT images in the database.

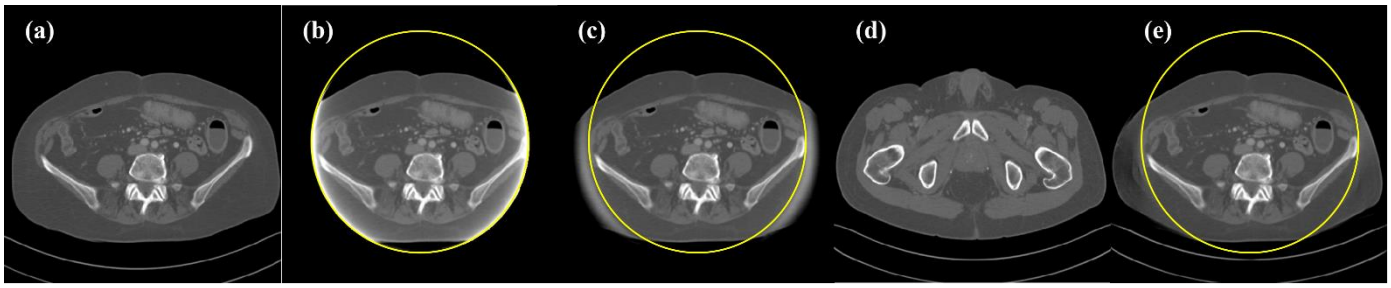

Fig. 5. Results of truncation artifact reduction. (a) The ground truth image; (b) image reconstructed from truncated projection without correction, with the FOV highlighted; (c) Gaussian extrapolation corrected image; (d) reference image selected from the database; (e) corrected image obtained using the proposed method.